U.S. Department of Commerce
National Oceanic and Atmospheric Administration
National Weather Service
National Centers for Environmental Prediction

Office Note 450

ASYMPTOTIC SOLUTION OF LIQUID WATER CONTENT EQUATION AT EQUILIBRIUM STATE OF RADIATION FOG

Binbin Zhou*

SAIC/Environmental Modeling Center,
National Centers for Environmental Prediction

March 16, 2006

* Correspondent author address: NCEP/Environmental Modeling Center, 5200 Auth Road, Camp Springs, MD 20746, U.S.A.; E-mail: Binbin.Zhou@noaa.gov ; Telephone: 301-763-8000 ext 7577

ABSTRACT

The liquid water content equation at a state of equilibrium for radiation fog was asymptotically solved with the *singular perturbation* technique. This report presents the detailed solution procedures, sensitivity testing of related parameters and discussions. The asymptotic solution describes the vertical structure of liquid water content which explicitly reveals the balance relationship between various factors in a steady radiation fog. It shows that cooling produces liquid water, which is regulated by droplet gravitational settling, while turbulence consumes the produced liquid water. The asymptotic solution also reveals that there exists a surface turbulence sub-layer, or *fog boundary layer (FBL)* within a radiation fog. The characteristic FBL depth is thinner for weaker turbulence and a larger cooling rate, whereas, if turbulence increases or the cooling rate decreases the FBL will develop from the ground. Through the FBL, a *critical turbulence exchange coefficient* for radiation fog was identified. This parameter is most interesting because it defines the upper bound of turbulence that a steady radiation fog can withstand. The deeper a fog is, the stronger a turbulence intensity it can endure, which explains why turbulence hinders or disperses a shallow fog near the ground but promotes a deeper fog at higher altitudes. Furthermore, the conditions for maintaining the state of equilibrium in a radiation fog can be characterized by either the critical turbulence exchange coefficient or the characteristic FBL depth . If turbulence decreases to below the critical turbulence intensity fog will form, while if turbulence exceeds the critical turbulence intensity or if the characteristic FBL depth dominates most of the fog bank, the state of equilibrium will be broken, leading to the dissipation of the radiation fog. The breakdown of the equilibrium condition can be applied to forecasts as a criterion to diagnose the formation or dissipation of radiation fog.

1. Introduction

Surface visibility is crucial for aviation and land transportation safety. One of the reasons for a reduction in surface visibility is fog, particularly radiation fog, which accounts for a significant percentage of all fog events in the central region (Westcott 2004), northeast region (Tardif 2004, Croft 2006), and southern region of the United States (Croft 1997). Radiation fog is a specific boundary layer phenomenon occurring near the surface on calm and clear nights and persisting until the next morning. The mechanisms for its evolution are very complex and have been extensively

studied for almost a century (e.g. Taylor, 1917), and have continued to be of considerable interest over the last two decades. For instance, several comprehensive observation programs and *in-situ* measurements were conducted in the 70's and the 80's (e.g. Roach 1976, Pinnick 1978, Jiusto 1980, Gerber 1981, Meyer 1986, Fitzjarrald 1989) and a series of numerical simulations were performed recently (Brown 1976, Welch 1986, Turton 1987, Zhou 1987, Bott 1990, Duynkerke 1991, 1999, Bergot 1994, Glasow 1999, Meyer 1999, Pagowski 2004, Muller 2005, etc.). The field studies and numerical simulations have greatly improved our knowledge of radiation fog, including the roles of radiation, droplet gravitational settling, nocturnal stratus clouds, and quasi-periodic oscillations, etc. However, some other factors have still no clear answers. The most controversial factor is the role of turbulence in the evolution of radiation fog. Some researchers have suggested that turbulence prevents the formation of radiation fog (Roach 1976). But others have supported the theory of turbulent mixing (e.g. Rodhe 1962) and argued that the formation and development of a radiation fog are associated with turbulence (Jiusto 1980, Welch 1986). Despite these observations and numerical simulations, no one opinion can be completely confirmed and exclusively accepted. Right now just one thing is known for sure, that radiation fog is a (turbulence) threshold event. In other words, only when turbulence intensity decreases below a certain threshold, can a radiation fog form near the ground. But the value for such a turbulence threshold is so far still a mystery and its subtle impact on the evolution of radiation fog is ambiguous. Another unknown feature is the "*equilibrium state*" or "*steady state*" of radiation fog. This particular state of radiation fog has long been noticed in the observations (e.g. Jiusto 1981). Such a state may be controlled by certain balance mechanisms between radiation and other factors, such as turbulence (Roach 1995). How the various factors interplay at the equilibrium state, and how they control the balance are still not understood. In order to answer these fundamental questions, this study will concentrate on the steady or equilibrium state of radiation fog. It will be seen in later sections that the balance mechanisms of a steady radiation fog are closely related to the problem of determining the turbulence threshold value.

The equilibrium state of a radiation fog can be understood from the apparent feature observed in detailed observations: that the evolution of a radiation fog, from its formation to its conditioning, maturity and dissipation, happens in stages (Figure 1.). Within each stage the fog bank, including

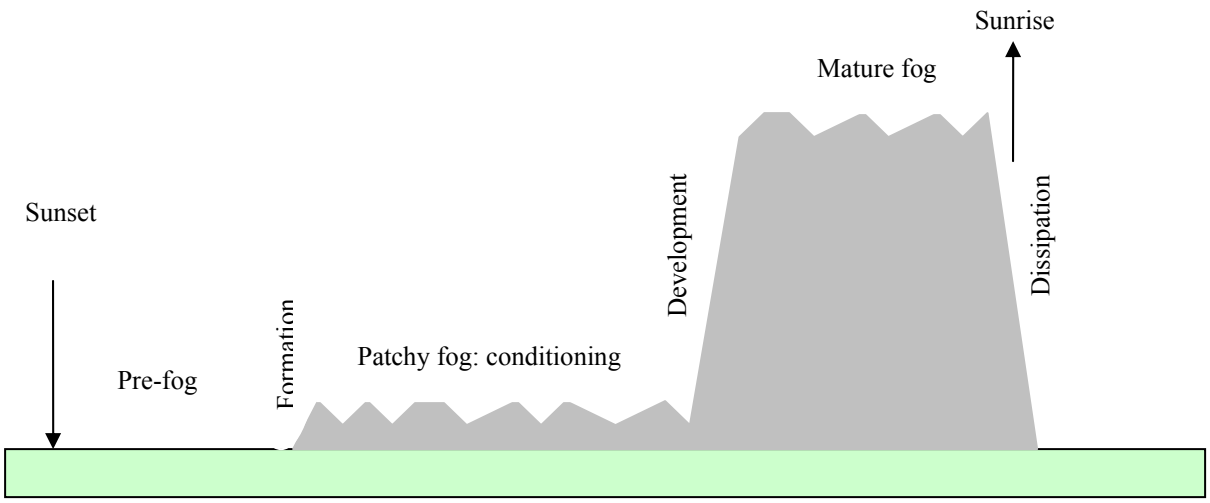

Fig.1: Conceptual diagram of typical stages in the evolution of radiation fog.

its depth, liquid water content (LWC), and droplet size distributions are in a certain *equilibrium* or *quasi-equilibrium* balance, while the transition between each stage appears to be quite fast. After a transition is finished, usually the fog rapidly stabilizes in its new stage. In the conditioning stage, a prominent phenomenon is *patchy ground fog* (Jiusto 1981). A patchy ground fog is usually very shallow and in most cases is restricted to the lowest 1-2 meters, but it can linger for several hours before it eventually either develops into a mature fog bank or disappears. A mature fog phase also shows a steady state which can maintain itself for a long period of time before sunrise. For example, some dense radiation fogs occurring in Chicago in the winter time can last for several hours after daybreak, since the morning solar radiation is too weak to disperse the fog layers (Friedlein 2004). The long period of stable stages in radiation fog implies that there exists a certain balance and a kind of "*self-maintenance*" mechanism inside a steady fog. It is evident that the development or disappearance of a patchy fog is the result of the breakdown of this balance as one or more variables suddenly change, for instance, the fluctuation of turbulence associated with an increase or decrease in wind speed, or a variation in cooling rate associated with nocturnal stratus clouds. If the breakdown is favorable for the development of fog, the patchy fog will grow rapidly, otherwise, a mature fog will not form. Statistics indicate that about 40 ~ 50% of patchy fogs eventually developed into mature fogs before morning (Meyer 1990). Other evidence showed that solar radiation is the major reason for the dispersal of mature fogs in the morning (Brown1976, Musson-Genon 1987, Bott 1990). Before sunrise, there is indeed some turbulent mixing developing from the

ground in a mature fog. However, such interior self-developed turbulence is too weak to break the equilibrium of a mature fog.

From the discussion above, it is anticipated that an examination of equilibrium states in radiation fog is an alternative way to understand or even predict radiation fog. A fog forecast is in essence the prediction of a temporally or spatially averaged visibility range that meets the definition of foggy conditions. Since a fog's visibility range can be solely related to its LWC (Kunkel 1984), if the distribution of LWC and the equilibrium conditions for a steady radiation fog exist, the forecast of fog will then become a diagnosis of the maintenance or breakdown of the equilibrium conditions for a steady fog, which is much simpler than forecasting fog itself. The purpose of this study is to seek the expressions for formulations of LWC and the balance conditions for steady radiation fog. The starting point of this study is solving the LWC equation for the equilibrium state of radiation fog, while the other variables such as wind, temperature, and humidity are treated as background, which simplifies the solving procedure.

A common belief is that radiation fog forms, develops, and exists in a weak turbulence environment associated with a very stable surface layer caused by strong cooling of the ground. In a weak turbulence environment, the liquid water content equation is a typical problem for the *singular perturbation* (see next section). The singular perturbation, an asymptotic analysis approach, was first suggested by Prandtl to solve the motion of an incompressible fluid with a large Reynolds number passing an object, and has since then been extended and widely applied in other scientific and engineering fields (Kelly 1994). In atmospheric science, this method was explored, for example, to investigate Ekman flow in the neutral barotropic planetary boundary layer (Blackadar 1968). In the present study, the singular perturbation technique was successfully applied in solving the LWC equation under steady fog conditions. The advantage of an analytic approach is that the solution is explicit, and the relationship between all of the important factors responsible for a steady fog can be directly and quantitatively examined. In the following sections, the procedure to solve the LWC equation is presented in detail, followed by the sensitivity test. Then the dynamic balance and the critical turbulence exchange coefficient will be discussed. Finally, the accuracy and uncertainties of the asymptotic solution as well as its potential application to forecasts are briefly discussed.

2. LWC equation for steady radiation fog

Under a steady flow, K-closured turbulence, and horizontally uniform conditions without considering evaporation, the governing equations for a steady radiation fog can be written as

$$\frac{\partial u}{\partial t} = 0 \quad \text{and} \quad \frac{\partial v}{\partial t} = 0 \tag{1}$$

$$\frac{\partial W}{\partial t} = \frac{\partial}{\partial z}(k\frac{\partial W}{\partial z}) - \frac{\partial G}{\partial z} - S + C = 0 \tag{2}$$

$$C = -\frac{\partial q_s}{\partial t} = -\frac{1}{p}\frac{de_s}{dT}(\frac{\partial T}{\partial t}) \tag{3}$$

$$\frac{\partial T}{\partial t} = -\frac{1}{\rho C_p}(\frac{\partial R_n}{\partial z}) - \frac{\partial}{\partial z}(k\frac{\partial \theta}{\partial z}) - \frac{L}{C_p}C \tag{4}$$

where u and v are the u and v components of wind speed, respectively. W is the liquid water content, in $g\ gk^{-1}$ and G is the droplet gravitational settling flux. C is the vapor condensation rate and q_s and e_s are the saturation specific humidity and pressure, respectively. p is the air pressure and T is the temperature. $\partial T / \partial t$ is the local total cooling rate. θ is the potential temperature and R_n is the net radiative flux. ρ, C_p and L are the air density, heat capacity and the latent heat of condensation, respectively. k is the turbulence exchange coefficient, which can be derived from profiles of wind and temperature (K-theory).

Fog layers are assumed to be saturated and the total water (liquid and vapor) is always conserved, so a decrease in temperature (cooling) will result in a reduction in the saturation specific humidity of the air and the excess will give rise to condensation as expressed by (3). The slope de_s / dT can be determined by the Clausius-Clapeyron equation, given the temperature and pressure.

The analysis of observation data suggested that after the early-evening transition of the surface layer, the layer-averaged temporal curvature of temperature $\partial^2 T / \partial t^2$ approaches zero, leading to an approximately constant local total cooling rate over time (Fitzjarrald 1989). For sake of simplicity, the total cooling rate $\partial T / \partial t$ is assumed to be a static distribution within a steady fog in this procedure.

The term S in Eq. (2) is the scavenging rate by the surface vegetation, including the direct impaction and capture of fog droplets by canopy leaves, which is proportional to the surface wind, leaf area index (LAI), liquid water content and efficiency of impaction (Shuttleworth 1977). In the

present study, the vegetation scavenging effect is not considered so that $S = 0$ is assumed. Since the fog layer under study is steady, $\partial W / \partial t$ is approximately zero, as a result, equation (2) becomes a second-order ordinary differential equation (ODE),

$$\frac{d}{dz}(k\frac{dW}{dz}) - \frac{dG}{dz} + \frac{1}{p}(\frac{de_s}{dT})C_o(z) = 0 \tag{5}$$

where the term $1/p(de_s/dT)C_o(z)$ is the condensation rate per unit mass of air due to cooling of the fog layers. The slope term, $1/p(de_s/dT)$, can be expressed by Clausius-Clapeyron equation as

$$\beta(p,T) = \frac{1}{p}(\frac{de_s}{dT}) = \frac{622L_v e_s(T)}{R_v T^2 p} \tag{6}$$

where L_v and R_v, are the latent heat for vapor and vapor constant, respectively. $C_o(z) = -(\partial T / \partial t)$ is the total cooling rate of the air, hereafter referred to as the cooling rate (positive for temperature decreases and negative for temperature increases). In general, the cooling rate has different vertical distribution patterns during the various development stages in fog.

k is the turbulence exchange coefficient. Because the present study is confined to the layers close to the surface k is hypothesized to be a small value without variation in height, allowing us to examine a steady fog in an average turbulence environment.

The droplet gravitational settling flux G can be parameterized as

$$G = v_t W \tag{7}$$

where v_t is the average droplet terminal velocity. The value of v_t depends on the droplet spectrum and can be derived from the Stokes terminal velocity law. For simplicity, v_t can be linearly related to LWC by a constant in the following

$$v_t = -\alpha W \tag{8}$$

The negative sign indicates that the settling is down towards the ground. For radiation fog, the observation data fitting suggested by Brown et al. (1976) shows that $\alpha = 0.062$ in ms^{-1}.

Assume that the fog depth is H with two boundary conditions where $W(0)=0$ and $W(H)=0$. The lower boundary condition means that the ground is a pure water droplet absorbing surface due to either settling or turbulence diffusion. Based on the above assumptions, Eq. (5) as well as boundary conditions can be written as the following boundary-value problem with a small parameter k :

$$k\frac{d^2W}{dz^2} + 2\alpha W\frac{dW}{dz} + \beta(T,p)C_o(z) = 0$$
$$W(0) = 0, W(H) = 0 \qquad (9)$$

Equation (9) is a non-linear, second-order ordinary differential equation which controls the interaction and balance between the turbulence, droplet gravitational settling and cooling in a steady radiation fog. In the singular perturbation notation, the small parameter is usually expressed as "ε". But in Eq. (9), the parameter is the turbulence exchange coefficient that is usually symbolized as uppercase K. Since we are considering the case of a weak turbulence environment, the lowercase k is used instead.

Before solving equation (9), a vertical distribution of cooling rate $C_o(z)$ must be assumed. The cooling rate is the residual of divergence of turbulent heat flux and radiative flux in fog, and depends on the stage of fog development. In the early stage when the fog layer is still optically shallow, the total cooling is nearly uniform within the shallow fog. In a dense fog, as a result of interaction between fog layers and radiation the maximum total cooling is located near the fog top, while in the lower part there is a slight warming (Roach 1976, Fitzjurrald 1989). We first assume the cooling rate is vertically uniform and solve the LWC equation to show the procedure for the overall solution, hereafter, a linearly distributed cooling rate is employed for general situations.

Both field observations and numerical simulations indicate that the favorable range of k for a radiation fog is typically ~ 10^{-2} m^2s^{-1} in the early stages and increases to around 10^{-1} m^2s^{-1} in the mature stage (Lala 1975, Roach 1976). For such a small value of k (10^{-2} ~ 10^{-1} m^2s^{-1} in radiation fog), equation (9) can be solved with the *singular perturbation* method (Van Dyke 1964). Here the "singular" means that when k = 0 in (9), Eq. (9) will become an one-order ODE. In this case, it satisfies only one of boundary conditions, while the other one is the singular point. The idea of a

singular perturbation is that, in the case of a small parameter, when a regular perturbation series may not match all the boundary conditions for a differential equation, there probably exists one or more regions where the solution varies rapidly. The procedure is to attempt to first find a solution in the form of a regular perturbation series by setting the parameter k to zero, which is called a "reduced problem". If a solution for the reduced problem exists, this solution is called the "outer" solution. The outer solution can only be satisfied by one boundary condition, not by another boundary condition which is called the "angular" or non-uniform convergent point. The angular point is then tested by covering a "*Prandtl's boundary layer*" where the solution varies rapidly, which is also called a transition region. Within the transition region, the solution is independent of the outer scale, z. Technically, the transition region is re-scaled by an inner scale $\tau = z/k$. Using this new scale, we solve the problem to obtain a so-called "inner" solution within the boundary layer. The inner and outer solutions must match somewhere in the transition region. If the inner solution is tested and transits smoothly to the outer solution while crossing the transition region (matching conditions), then the final solution can be constructed from both the inner and the outer solutions.

Where the boundary layer is placed, at the upper bound (fog top, $z = H$) or at the lower bound (surface, $z = 0$), depends upon mathematical or physical considerations. Here, a practical rule suggested by O'Malley (1974) can be easily employed for a second-order ODE: if the coefficient term ($2\alpha W$) is positive for the whole domain one must select "$z = 0$" as a non-uniform convergent point in order to satisfy the matching principle, while for a negative coefficient term, select "$z = H$" as the point. Obviously, $2\alpha W$ is always a non-negative value, that is, the fog droplets deposit on the ground (as a result of the gravity effect) where a boundary layer will form. Therefore, the lower bound as a non-uniform convergent point is selected for the LWC equation. As a result, the outer equation picks up only the upper boundary condition and no longer satisfies the lower boundary condition.

Let us first search for the outer solution, W_{out}, which is assumed as a formal asymptotic expansion series:

$$W_{out}(z,k) \sim \sum_{j=0}^{\infty} k^j \eta_j(z) \qquad (10)$$

Substitute (10) into (9), have following general expression:

$$
\begin{aligned}
&(2\alpha\eta_0 \frac{d\eta_0}{dz} + \beta C_o) + \\
&k(\frac{d^2\eta_0}{dz^2} + 2\alpha\eta_0 \frac{d\eta_1}{dz} + 2\alpha\eta_1 \frac{d\eta_0}{dz}) + \\
&k^2(\frac{d^2\eta_1}{dz^2} + 2\alpha\eta_0 \frac{d\eta_2}{dz} + 2\alpha\eta_1 \frac{d\eta_1}{dz} + 2\alpha\eta_2 \frac{d\eta_0}{dz}) + \\
&\text{.....} \\
&= 0
\end{aligned}
\tag{11}
$$

Or

$$
(2\alpha\eta_0 \frac{d\eta_0}{dz} + \beta C_o) + \sum_{n=1}^{\infty} k^n (\frac{d^2\eta_{n-1}}{dz^2} + 2\alpha \sum_{i,j=0}^{i+j=n} \eta_i \frac{d\eta_j}{dz}) = 0 \tag{12}
$$

when $k \to 0$ and considering the upper boundary condition, we have following reduced differential equation:

$$
\begin{aligned}
&2\alpha\eta_0 \frac{d\eta_0}{dz} + \beta C_o = 0 \\
&\eta_0(H) = 0
\end{aligned}
\tag{13}
$$

The general solution of (13) is

$$
\eta_0^{\,2} = \frac{\beta C_o z}{\alpha} + C_1 \tag{14}
$$

where C_1 is an integration constant. Using the upper boundary condition, we have $\frac{\beta C_o H}{\alpha} + C_1 = 0$, or

$$
C_1 = -\frac{\beta C_o H}{\alpha} \tag{15}
$$

Therefore, the solution for (13) is

$$
\eta_0(z) = [\frac{\beta C_o}{\alpha}(H - z)]^{1/2} \tag{16}
$$

Thus, the outer solution for (9) can be written as

$$W_{out}(z,k) = [\frac{\beta C_o H}{\alpha}(1-\frac{z}{H})]^{1/2} + O(k) \quad , z > 0 \tag{17}$$

Obviously, equation (17) is not satisfied by the lower boundary condition $W(0) = 0$.

Now let us look at the inner solution within the boundary layer and try to match both the outer and inner solutions near the lower bound. Replacing the inner scale $\tau = z/k$ in (9), we have

$$\frac{d^2W}{d\tau^2} + 2\alpha W\frac{dW}{d\tau} + k\beta C_o = 0 \tag{18}$$

Suppose the inner solution also has the form of the following formal asymptotic expansion series

$$W_{in}(\tau,k) \sim \sum_{j=0}^{\infty} k^j \xi_j(\tau) \tag{19}$$

In the singular perturbation technique, there are several formal methods to match the outer and inner solutions. The most often used is "matching" (Van Dyke 1964). The matching method suggested by Van Dyke needs to find the outer and inner solutions first and then matches them with some matching constraints. This is particularly difficult for the present case in that we have to find the explicit formulation for the inner solution at first. Thus, we employ another approach called the "*layer correction"* methodology, suggested by O'Malley (1974), which has proved more convenient for the present study. The layer correction enforces the matching conditions on the inner equation in addition to the boundary condition at the non-uniform convergent point. The procedure for the layer correction method is to first construct the whole solution by combining the outer solution and the inner solution such that

$$W(z,k) = W_{out}(z,k) + W_{in}(\tau,k) \tag{20}$$

The matching conditions are that, if and only if both $W_{in}(\tau,k)\to 0$ and $dW_{in}(\tau,k)/d\tau\to 0$ as $\tau\to\infty$, then $W(z,k)\to W_{out}(z,k)$ smoothly as the scale z crosses the transition region from the lower bound.

By substituting (10), (19) and (20) into (11), we have following dual-scale equation:

$$k^2\frac{d^2W_{out}(z,k)}{dz^2}+\frac{d^2W_{in}(\tau,k)}{d\tau^2}+2\alpha[W_{out}(k\tau,k)+W_{in}(\tau,k)]\frac{dW_{in}(\tau,k)}{d\tau}$$
$$+2k\alpha[W_{out}(z,k)+W_{in}(\tau,k)]\frac{dW_{out}(z,k)}{dz}+k\beta C_o=0 \qquad (21)$$

Since the outer solution $W_{out}(z, k)$ also satisfies Eq (9), (21) must have the following form:

$$\frac{d^2W_{in}(\tau,k)}{d\tau^2}+2\alpha[W_{out}(k\tau,k)+W_{in}(\tau,k)]\frac{dW_{in}(\tau,k)}{d\tau}+2k\alpha W_{in}(\tau,k)\frac{dW_{out}(z,k)}{dz}=0 \qquad (22)$$

set $k\to 0$, and the following inner equation is reached:

$$\frac{d^2W_{in}(\tau,0)}{d\tau^2}+2\alpha[W_{out}(0,0)+W_{in}(\tau,0)]\frac{dW_{in}(\tau,0)}{d\tau}=0 \qquad (23)$$

Substituting the asymptotic expansions for both the inner and outer solutions, i.e., Eqs (10) and (19) are substituted into (23) and $k = 0$, the reduced solution ξ_0 for the inner equation becomes

$$\frac{d^2\xi_0(\tau)}{d\tau^2}+2\alpha[\eta_0(0)+\xi_0(\tau)]\frac{d\xi_0(\tau)}{d\tau}=0 \qquad (24)$$

The lower boundary condition for the inner solution is

$$\xi_0(0)=0-\eta_0(0)=-\left(\frac{\beta C_o H}{\alpha}\right)^{1/2} \qquad (25)$$

With Leibnitz's integration formula $\frac{d}{dx}\int_0^{f(x)} y(x')dx' = y[f(x)]\frac{df(x)}{dx}$, (24) is transformed to

$$\frac{d^2\xi_0(\tau)}{d\tau^2} + \frac{d}{d\tau}\int_0^{\xi_0(\tau)} 2\alpha[\eta_0(0) + \tau']d\tau' = 0 \tag{26}$$

Integrating both terms in (26) once, we have

$$\frac{d\xi_0(\tau)}{d\tau} + \int_0^{\xi_0(\tau)} 2\alpha[\eta_0(0) + \tau']d\tau' + C_2 = 0 \tag{27}$$

Where C_2 is an integration constant. Under the matching conditions $\lim_{\tau\to\infty}\frac{d\xi_0}{d\tau} \to 0$ and $\lim_{\tau\to\infty}\xi_0 \to 0$, (27) will become

$$0 + \int_0^0 2\alpha[\eta_0(0) + \tau']d\tau' + C_2 = 0 \tag{28}$$

Then C_2 in (28) must be zero. Integrating the second term in (27) further, we have

$$\frac{d\xi_0(\tau)}{d\tau} + 2\alpha[\eta_0(0)\xi_0(\tau) + \frac{1}{2}\xi_0^2(\tau)] = 0 \tag{29}$$

The (29) can be re-arranged as

$$\frac{d\xi_0}{2\eta_0(0)\xi_0 + \xi_0^2} = -\alpha d\tau \tag{30}$$

Solving (30), we have

$$\frac{1}{2\eta_0(0)}\ln\frac{2\eta_0(0) + \xi_0(\tau)}{\xi_0(\tau)} = \alpha\tau + C_3 \tag{31}$$

Or

$$\ln \frac{2\eta_0(0) + \xi_0(\tau)}{\xi_0(\tau)} = \alpha \eta_0(0)\tau + C_3 \tag{32}$$

Or

$$\frac{2\eta_0(0) + \xi_0(\tau)}{\xi_0} = C_3 e^{2\alpha\eta_0(0)\tau} \tag{33}$$

where C_3 is an integration constant. With the lower boundary condition (25), C_3 = -1. Then we obtain the solution for ξ_0 :

$$\xi_0(\tau) = -\frac{2\eta_0(0)}{1 + e^{2\alpha\eta_0(0)\tau}} \tag{34}$$

Then we have the inner solution

$$W_{in}(\tau, k) = -\frac{2\eta_0(0)}{1 + e^{2\alpha\eta_0(0)\tau}} + O(k) \tag{35}$$

Since both α and $\eta_0(0)$ are positive, it can be easily tested to show that when $\tau \to \infty$, both $W_{in}(\tau, k) \to 0$, and $dW_{in}(\tau, k)/d\tau \to 0$. So the inner solution satisfies the matching conditions for layer correction. The entire solution can then be uniquely obtained by combining (17) and (35) together as

$$W(z,k) = [\frac{\beta C_o H}{\alpha}(1 - z/H)]^{1/2} - \frac{2\eta_0(0)}{1 + e^{2\alpha\eta_0(0)\tau}} + O(k) \tag{36}$$

Omitting the terms with a higher order of *k* and substituting $\tau = z/k$, we obtain the final asymptotic solution for the liquid water content equation:

$$W(z,k) = [\frac{\beta C_o H}{\alpha}(1 - z/H)]^{1/2} - \frac{2\eta_0(0)}{1 + e^{2\alpha\eta_0(0)z/k}} \tag{37}$$

Since the inner solution satisfies the matching requirement, as $z >> 0$, the whole solution will approach the first term or the outer solution. On the other hand, as $z \to 0$, it can be easily verified that equation (37) will approach zero, satisfying the lower boundary condition, $W(0) = 0$.

It can be observed from (37) that three factors control the LWC structure of a steady radiation fog: (i) cooling rate C_o, which is needs to be positive (continuously decreasing in temperature) to produce the liquid water; (ii) droplet gravitational settling parameter α, which acts as a regulator to adjust the cooling-produced LWC in the first term; and (iii) turbulence, represented by the inner solution in equation (37). It is of interest to note that the turbulence term has a negative contribution, implying that turbulence always depletes the cooling-produced liquid water inside the fog layers. Since the turbulence term (inner solution) is significant near the surface, the depletion of fog water only happens in the lower part of the fog except when the value of *k* is very large. From (37), it appears that the characteristic depth of a turbulence sub-layer within a fog layer can be defined as:

$$\delta = \frac{k}{2(\alpha\beta C_o H)^{1/2}} \tag{38}$$

The turbulence sub-layer can be thought of as a *fog boundary layer* (FBL) and is a function of the turbulence intensity, cooling rate, droplet gravitational settling and fog depth. For weak turbulence and a large cooling rate, δ is small, while as the turbulence increases or cooling rate decreases, it will develop up from the surface. Such behavior is similar to the surface mixing layer observed in mature radiation fog (see our later discussion).

With the definition of (38), equation (37) can be re-arranged as

$$W(z,k) = (\frac{\beta C_o H}{\alpha})^{1/2}[(1-\frac{z}{H})^{1/2} - \frac{2}{1+e^{z/\delta}}] \tag{39}$$

Equation (39) means that the influence of turbulence on the distribution of LWC is controlled by the dimensionless parameters *z/H* and z/δ. Further integrating over the entire fog depth, we can obtain the average liquid water content W_a of the fog bank:

$$W_a = \frac{1}{H}\int_0^H W(z,k)dz = (\frac{\beta C_o H}{\alpha})^{1/2}[\frac{1}{H}\int_0^H (1-z/H)^{1/2}dz - \frac{2}{H}\int_0^H \frac{dz}{1+e^{z/\delta}}] \qquad (40)$$

In (40), the first integration is $\int_0^1 (1-x)^{1/2}dx = -2/3(1-x)^{2/3}\,|_0^1 = 2/3$. The second integration is

$$\frac{2\delta}{H}\int_0^{H/\delta} \frac{dt}{1+e^t} = \frac{2\delta}{H}(\ln\frac{e^t}{1+e^t}\,|_0^{H/\delta}) = \frac{2\delta}{H}\ln\frac{2e^{H/\delta}}{1+e^{H/\delta}} \qquad (41)$$

It will be shown in the later sections that in most cases, $\delta <<$ H. Then (41) can be approximately estimated by

$$\frac{2\delta}{H}\lim_{x\to\infty}\{\ln\frac{2e^x}{1+e^x}\} \approx \frac{2\delta\ln 2}{H} \qquad (42)$$

Thus, we have

$$W_a \approx \frac{2}{3}(\frac{\beta C_o H}{\alpha})^{1/2} - \frac{k\ln 2}{\alpha H} \qquad (43)$$

Equations (39) and (43) demonstrate that both LWC and the averaged liquid water content of a steady radiation fog ~ $C_o^{1/2}$ and $H^{1/2}$. The first term on the right hand side of (43) is the controlling term, contributed to by cooling and regulated by gravitational settling; the second is the turbulence depletion term. Again, the turbulence term has a negative contribution to the average LWC. Because the parameter β is a function of temperature and pressure, the liquid water content W in (39) and W_a in (43), in turn, depend on temperature and pressure as well. Equations (39) or (43) have confirmed the *balance* assumption for radiation fog suggested by Roach (1995) that a fog is controlled by a balance between (radiative) cooling and turbulence. What the balance condition is and how such a balance is controlled will be discussed in the later sections.

The above solution is for a uniform cooling rate. In general, the cooling rate is not uniformly distributed as previously mentioned, particularly in dense fogs. Now assume that the cooling rate follows a linear vertical distribution within a steady fog: $C_o(z) = C_b + (C_t - C_b)z/H$, where C_b is

the temperature variation at the bottom (> 0 for cooling and <0 for heating) and C_t is the cooling rate at the fog top (H). Such an assumption may not precisely represent the real situation within the fog layers. However, it is simple and represents the general pattern for the cooling rate in radiation fog. By using this linearly distributed cooling rate and repeating the above methodology, we have the reduced outer equation

$$\begin{aligned} &2\alpha\eta_0 \frac{d\eta_0}{dz} + \beta(C_b + \frac{C_t - C_b}{H} z) = 0 \\ &\eta_0(H) = 0 \end{aligned} \tag{44}$$

The trivial solution of (44) is

$$\eta_0(z) = [\frac{\beta(C_b + C_t)H}{2\alpha}]^{1/2} \{ [1 - \frac{2C_b}{(C_b + C_t)} \frac{z}{H} + \frac{(C_b - C_t)}{(C_b + C_t)} (\frac{z}{H})^2]^{1/2} \} \tag{45}$$

The inner solution has the same format as the equation (35), so we have the entire solution

$$W(z,k) = [\frac{\beta(C_b + C_t)H}{2\alpha}]^{1/2} \{ [1 - \frac{2C_b}{(C_b + C_t)} \frac{z}{H} + \frac{(C_b - C_t)}{(C_b + C_t)} (\frac{z}{H})^2]^{1/2} - \frac{2}{1 + e^{z/\delta}} \} \tag{46}$$

where the characteristic depth of a turbulence sub-layer is defined as:

$$\delta = \frac{k}{[2\alpha\beta(C_b + C_t)H]^{1/2}} \tag{47}$$

The expression for average LWC is very complex and will not be presented here. But for a special case, where $C_b = C_t = C_o$, (46) and (47) will reduce to (39) and (43), respectively. For another special case, where $C_b = 0$, equations (46) and (47) become

$$W(z,k) = (\frac{\beta C_t H}{2\alpha})^{1/2} \{ [(1 - (\frac{z}{H})^2]^{1/2} - \frac{2}{1 + e^{z/\delta}} \} \tag{48}$$

where

$$\delta = \frac{k}{(2\alpha\beta C_t H)^{1/2}} \tag{49}$$

Integrating (48) over the entire fog bank:

$$W_a = \frac{1}{H}\int_0^H W(z,k)dz = (\frac{\beta C_t H}{2\alpha})^{1/2}[\frac{1}{H}\int_0^H [1-(z/H)^2]^{1/2}dz - \frac{2}{H}\int_0^H \frac{dz}{1+e^{z/\delta}}] \tag{50}$$

The first integration in (50) is

$$\frac{1}{H}\int_0^H [1-(z/H)^2]^{1/2}dz = \int_0^1 (1-x^2)^{1/2}dx = \frac{1}{2}[x(1-x^2)^{1/2} + \sin^{-1}(x)]\,|_0^1 = \frac{\pi}{4} \tag{51}$$

The second integration is approximately 2δ ln2/H (for δ << H). Thus, we have the average LWC:

$$W_a = \frac{\pi}{4}(\frac{\beta C_t H}{2\alpha})^{1/2} - \frac{k\ln 2}{\alpha H} \tag{52}$$

As we know, in dense fog the fog top is dominated by strong radiative cooling while the cooling near the surface is usually very small or even a slight warming. So, equations (46) and (52) can be applied in a dense fog to replace equations (45) and (47).

3. Sensitivity test and discussion

The asymptotic solution of the LWC equation is analytical and simple to use. An advantage of the analytical expressions of the asymptotic solution is that the roles of various factors in the formulations are explicit and can be quantitatively discussed. The formulations (39) through (52) indicate that the key factors having impacts on the LWC distributions or the average LWC of a

steady radiation fog are cooling rate, gravitational settling, and turbulence or the characteristic depth of the fog boundary layer. How these factors affect the LWC computation can be directly examined with these formulations. Furthermore, the balance conditions and turbulence threshold for a steady radiation fog can conveniently be identified as well.

a. Outer solution, inner solution and turbulence

We have seen that the solution for LWC at the equilibrium state of a radiation fog is composed of an outer and inner solution. The outer solution is controlled by cooling rate and droplet gravitational settling, while the inner solution is controlled by turbulence which is a negative contributor to the liquid water content. That means in the steady stages of a radiation fog, turbulence will exhaust the liquid water within the fog layers. The impact of turbulence on the distribution of LWC is presented in Figs. 2a and 2b, where the temperature is 0 ^{o}C, pressure p = 1000mb, fog top H = 30 m, the cooling rate is 1.0 $^{o}C\ hr^{-1}$, and turbulence exchange coefficient k = 0.01 $m^2\ s^{-1}$, which are typical values for a shallow radiation fog. Figure 2a shows that the turbulence has nothing to do with the outer solution but has a significant impact on the inner solutions. For a small turbulence exchange coefficient the inner solution rapidly decreases with the height, but for a large turbulence exchange coefficient the inner solution slowly approaches zero. Such behavior by the inner solution demonstrates that the inner solution usually dominates near the surface. Only after the turbulence intensity increases dramatically (associated, for instance, with solar radiation), can its affect reach the higher regions of the radiation fog. The LWC of the fog is in the area surrounded by both the outer solution and the inner solution, as shown in Fig. 2b, indicating that the larger the turbulence is the smaller the LWC will be. This reflects the depletion effect of turbulence on the fog water.

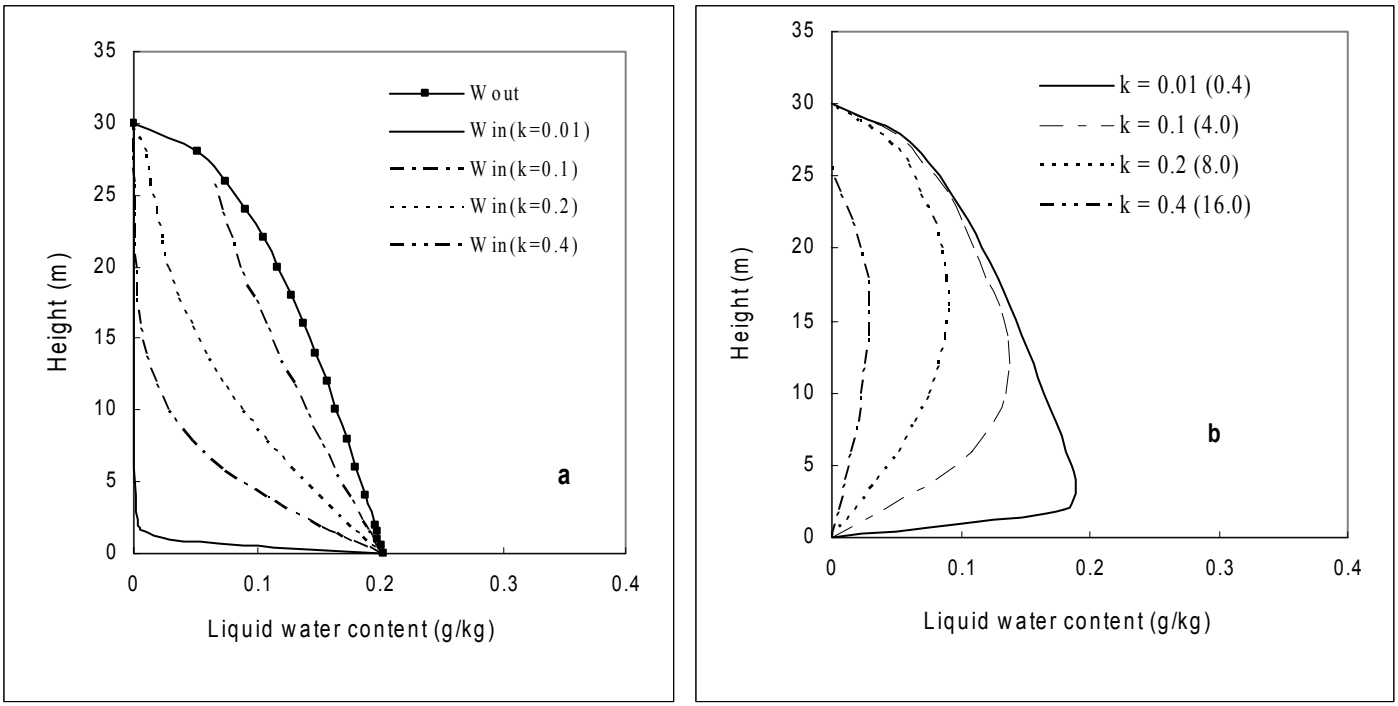

Fig. 2. (a) Outer solution and inner solution with different turbulence exchange coefficients, in $m^2 s^{-1}$, (b) Overall LWC distributions based on (a); the corresponding δ values, in m, are indicated in ( )

The input data in this example are very similar to the radiation fog event reported by Roach et al. (1976, Case A). In that particular fog the fog top remained thin, within 10 m of the ground, for about 3 hours before it rapidly developed into a 30 m mature fog. The mature fog bank lasted another 3 hours before it dispersed after sunrise. The temperature and the cooling rate in the radiation fog were reported to be about 0 ^oC and 1.0 $^oC\ hr^{-1}$, respectively. The turbulence exchange coefficient was estimated to be about 0.005 $m^2\ s^{-1}$ at the initial stage near the surface and 0.1 $m^2\ s^{-1}$ during the mature stage. The measured LWC at the lower levels ranged between 0.08 ~ 0.22 *g/kg*. Fig. 2b shows that the calculated LWC at the lower levels is around 0.1 ~ 0.2 *g/kg*, which is in good agreement with the measurements.

In an equilibrium state, LWC in a radiation fog is the result of the dynamic balancing of cooling, droplet gravitational settling, and turbulence as expressed by equations (39) or (46). In the turbulence cessation period, overall LWC is larger and the level of maximum LWC is located lower toward the surface (Fig. 2b). In this case, most condensed liquid water droplets deposit near the surface but yet are still not transferred to the surface. By contrast, if turbulence increases, LWC becomes smaller and the location of maximum LWC rises as a result of the rapid transfer of fog water to the ground. The stronger the turbulence is, the faster the fog water transfers. It can be

expected that if turbulence intensity is strong enough, the liquid water in fog layers will be completely exhausted. This is particularly true during the dissipation period when turbulence intensity is dramatically increased, due to either sunrise or clouds.

The average LWC equations (43) or (52) reveal another fact - that turbulence has less impact on dense fogs than shallow fogs since the turbulence term is reduced by a factor of *1/H*. This can be seen from Fig. 3, which compares the ratio of the turbulence contribution (inner solution) to the cooling contribution (outer solution) for different fog depths under different turbulence intensities. For example, we'll compare a 30 m shallow fog and a 100 m dense fog at a temperature of 0 ^oC. If k = 0.01 $m^2 s^{-1}$, the ratio is 3% for the shallow fog and 0.25 % for the dense fog. If k is increased to 0.1 $m^2 s^{-1}$, then the ratio increases to about 30% for the shallow fog but only 5 % for the dense fog. Such a conclusion appears to agree with the observations reported by Fitzjarrald et al. (1989), who found that a radiation fog can be classified as either a *surface layer fog* or a *boundary layer fog*. A surface layer fog is shallow and characterized by the dominant role of turbulence, while a boundary layer fog is deeper and primarily controlled by radiative cooling at the fog top.

It can be seen in Fig. 3 that for some larger turbulence coefficients, the ratio exceeds 1.0, which means the turbulence term is larger than the cooling term, in other words, the fog layer disperses completely. This will be discussed in later sections.

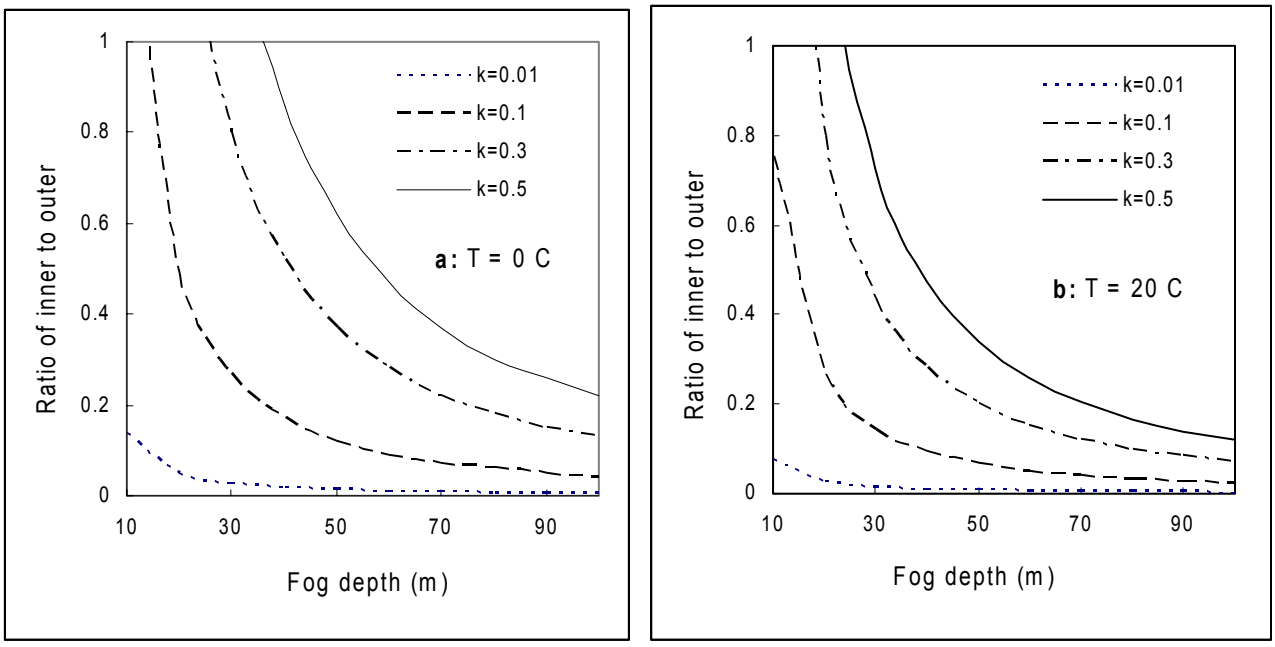

Fig. 3: The ratio of inner and outer solutions against different fog depths with the same cooling rate of 1 $^oC\ hr^{-1}$ but different temperatures: (a) T = 0 ^oC and (b) T = 20 ^oC.

b. Total cooling rate

The observations and numerical simulations have revealed that the most important contributions to cooling in nocturnal boundary layer are the convergence or divergence of radiative and turbulence fluxes near the surface. In the present study, both radiative and turbulent cooling are combined in the total cooling rate. That means the cooling rate presented in the LWC formulations is the net effect of these two contributions. After sunset, strong cooling in the surface layer due to heat loss from the ground leads to a rapid drop in temperature and the saturation of the air adjacent to the ground. A further decrease in the temperature the of saturated air will give rise to vapor condensation and the generation of fog. Once fog forms, cooling rate, as indicated by the solution, is the major engine that continuously generates liquid water droplets to maintain the steady fog layers. If the fog bank is shallow, strong cooling is still near the surface and the cooling rate measured near the surface approximately represents the overall value for the entire fog. But as the fog deepens, the cooling rate is not a vertically constant distribution since the area of strongest cooling rises to the fog top from the ground. As a result, the liquid water in the deep fog is largely generated in the upper regions of the fog and is transferred by either gravitational settling or turbulence to the ground. The LWC distribution formulations (46) or (48) describe such a mechanism in a deep fog. However, the cooling rate at the top of a deep fog is not readily detected without special equipment at high levels. A practical question is whether the simplified LWC formulation (48) or even the shallow fog formulation (39) can be applied in a deep fog.

To compare the different LWC formulations for a deep fog, three cooling rates are tested with the formulations (39), (46) and (48). The input data are selected similar to the deep fog reported by Roach et al. (1976, Case B). Like Case A, this deep fog also experienced a long shallow stage (2 hours) before it eventually grew to a fog more than 100m deep. The deep fog phase lasted 8 hours, much longer than that of the shallow fog in Case A. The temperature was around 0 ^{o}C. The observed cooling rate was 2 ~ 3 $^{o}C\ hr^{-1}$ at the fog top but with a slight warming (about 0.5 $^{o}C\ hr^{-1}$) near the ground. The turbulence exchange coefficient was in the range of 0.1 ~ 1.0 $m^2 s^{-1}$. The measured LWC at 4 levels (1m, 3m, 9m, and 28m) indicated that it ranged between 0.06 and 0.29 g m^{-3}. In the test, the three selected cooling rates were: (1) a constant rate of 1.0 $^{o}C\ hr^{-1}$, which represents a average cooling rate over all fog layers; (2) a linearly distributed cooling rate of 2.5 $^{o}C\ hr^{-1}$ at the fog top and a warming of 0.5 $^{o}C\ hr^{-1}$ at the bottom; (3) a linearly distributed cooling rate of 2.5 $^{o}C\ hr^{-1}$ at the fog top but with a zero rate at the bottom. The turbulence was set to 0.5 $m^2 s^{-1}$

for all three cases, representing an overall turbulence environment. The fog top was set at 150m, representing the average depth of the fog top. The calculated LWC distribution profiles with the three different cooling rates are compared in Fig. 4, which indicates a similarity in the LWC distribution pattern among the three cases with slight differences in the maximum LWC locations. The maximum values of the three LWC profiles have about a 20~30 % difference, which might be acceptable. The measurements of the LWC at higher levels are not available for this particular deep fog event. Nevertheless, the overall calculated LWC at the lowest levels is close to what was observed near the ground.

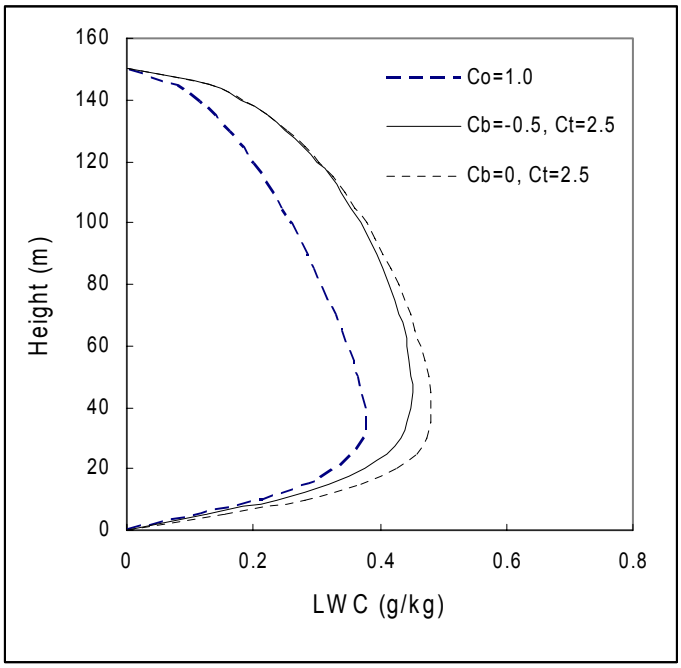

Fig. 4: LWC profiles for T=0 ^{o}C , p=1000 mb, H=150m, k=0.5 $m^2 s^{-1}$ but with different cooling rates: (1) constant (long dashed), (2) linear with cooling at the fog top and warming at the bottom (solid), (3) linear with cooling at the fog top but neutral at the bottom (dashed).

c. Droplet gravitational settling

Droplet gravitational settling was not considered in early fog studies or numerical simulations (e.g. Zdunkowski 1972, Oliver 1978). Its important role in the water budget of radiation fog was first revealed in field observations as well as in the numerical study by Roach et al. (1976) and Brown et al. (1976). They found that if the droplet gravitational settling was not included, the water budget and the modeled LWC will be unrealistically large and pointed out that the observed LWC in radiation fog was only a small percentage of the total condensation and that most of the condensed liquid water in fog deposited on the ground. Most current numerical fog models deal with droplet

gravitational settling by using a linear fit between terminal velocity and LWC as expressed in equation (8) suggested by Brown et al. (1976), although such a relationship actually depends on both liquid water and the total number of fog droplets (Corradini 1980). In this discussion, the linear relationship (8) is tested with different α values to evaluate its effect on the distribution of liquid water content.

Still using the first test case (Fig. 2) but with k set to 0.01 $m^2 s^{-1}$ and different α's of 0.001, 0.01, 0.03, 0.06, 0.09 and 0.12, the calculated average and distributions of LWC are illustrated in Figs 5 (a) and (b). The 0.001 α represents an underestimation of droplet gravitational settling. The results show that the parameter α has a significant impact on both LWC profile and average LWC. If α is too small, for instance, α = 0.001, the LWC profile has a maximum LWC value of 1.2 $g\ kg^{-1}$ and an average LWC of 0.8 $g\ kg^{-1}$. Only a convective cloud can reach such a high LWC amount, which is unrealistic in comparison to the 0.1 ~ 0.2 *g/kg* LWC range observed in radiation fog. When α increases to 0.03, the calculated LWC decreases sharply to the realistic range for radiation fog. As α increases further, both the profile and the average value of LWC vary little, indicating that the reasonable range for α is between 0.03 ~ 0.1. Such a range of α supports the coefficient 0.062 for the linear fit between LWC and mean terminal velocity of fog droplets suggested by Brown et al. (1976).

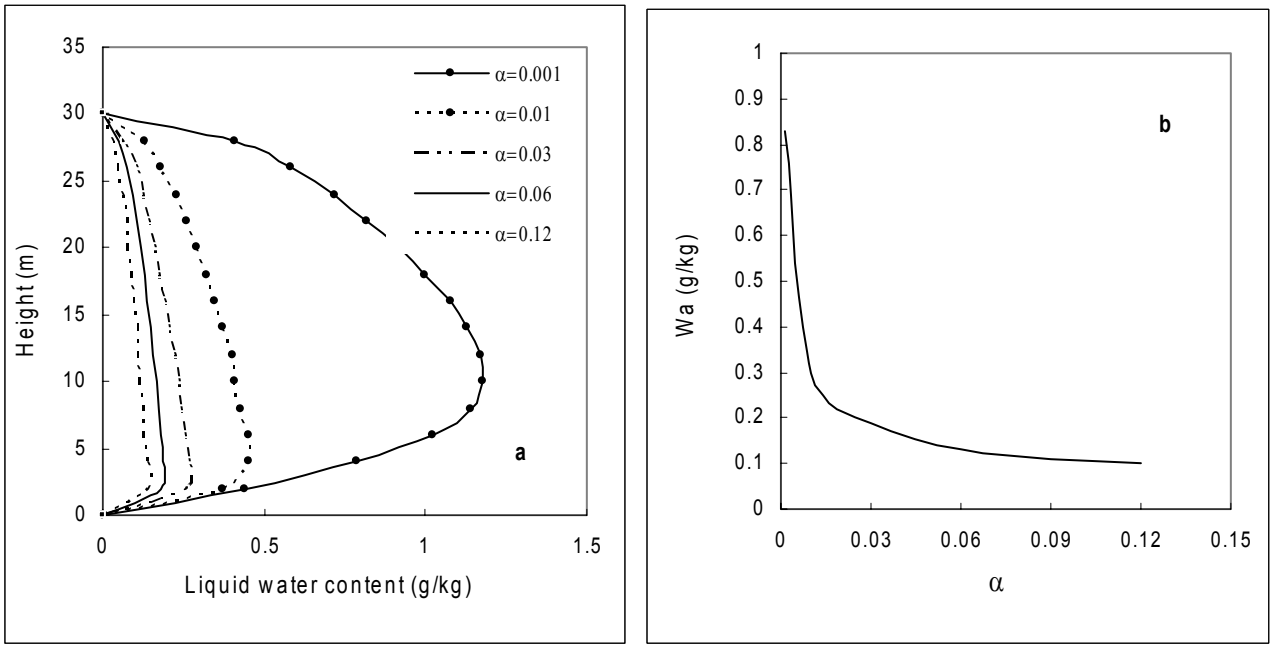

Fig. 5. LWC distributions (a) and average LWC (b) similar to Fig. 2 but for $k = 0.01\ m^2 s^{-1}$ and for different α values.

The value of α also affects the location of maximum liquid water content as shown in Fig 4(a). For a larger value of α, the maximum location is lower than that for a smaller α, reflecting the gravitational effect on the distribution of liquid water content within steady radiation fog layers.

d. Fog boundary layer (FBL)

The characteristic depth of a FBL, δ, is a function of turbulence, cooling rate and fog depth as defined in (38), (47) and (49), and is mathematically required for and defined from the LWC asymptotic solution in a steady radiation fog. The formation of a FBL inside a fog is the consequence of interactions between two media, the fog bank and the ground, as the first medium "flows" over the second under the influences of cooling, turbulence and gravity. If the cooling rate is adequate, a FBL will form on the ground but is thin in comparison with the entire fog bank. The magnitudes of δ for different temperatures, fog depths and turbulence exchange coefficients are plotted in Fig. 6.

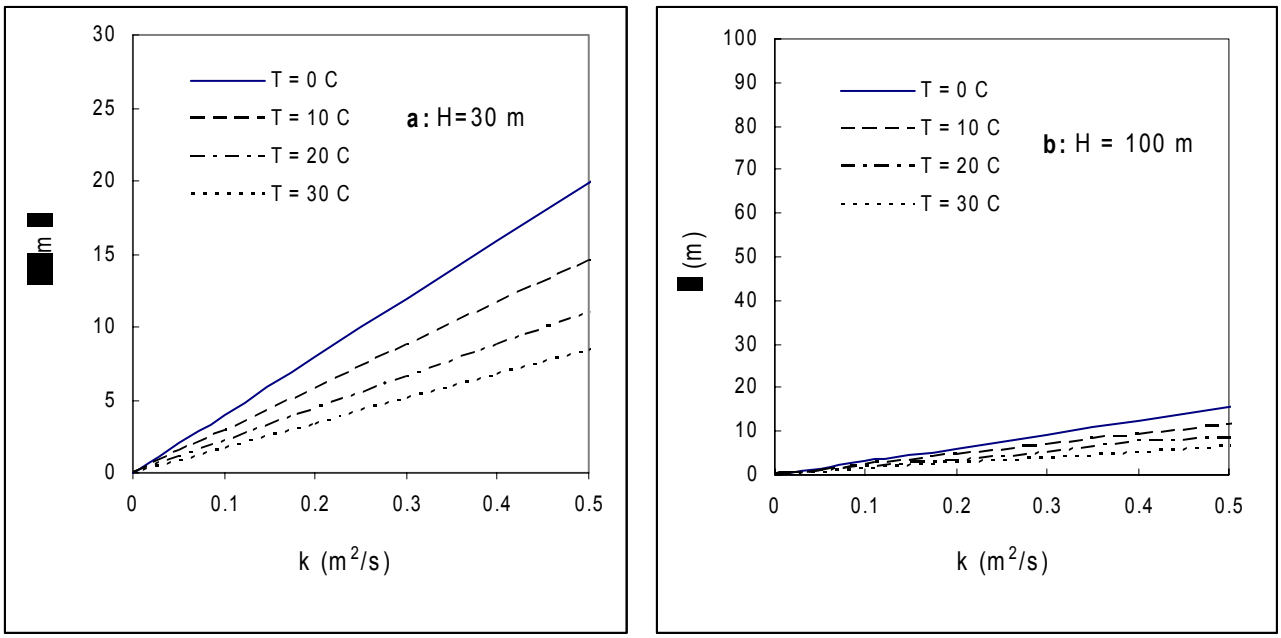

Fig. 6: The characteristic FBL depth for different turbulence exchange coefficients and different temperatures in a shallow (a) and a deep fog (b), respectively. The cooling rate is set to the typical value of 1 $^{o}C\ hr^{-1}$ in both cases.

For example, for a 30m deep fog with k = 0.01 m^2s^{-1}, δ has a value of 0.3 m, or 1% of the fog depth, while for a 100 m deep fog with k = 0.1 m^2s^{-1}, δ is about 3 m, or 3% of the fog depth. Such a percentage for δ is consistent with the depth of the unstable surface mixing layer suggested by observations and numerical simulations (e.g. Roach 1976, Brown, 1981, Musson-Genon, 1987). The observations showed that if the cooling rate within a fog is reduced or turbulence is strengthened for some reason (e.g. a cloud mass moves in or winds increase) the unstable surface mixing layer will develop from the bottom layers of fogs. A similar behavior in FBL can also be expected from equations (38) or (47). For example, if the cooling rate C_o in Eq. (38) is decreased or the warming rate C_t in Eq. (47) is increased, the characteristic depth of δ will increase. It appears that although the FBL is mathematically defined by the LWC asymptotic solution, it well represents the behavior of the temperature-related mixing layer near the surface observed in real radiation fogs.

e. Balance conditions for steady fog

As shown in equations (38)-(43) or (48)-(52), maintaining a steady fog requires a positive cooling rate inside the fog layers, that is, temperature, as a whole, steadily deceases with time in order to continuously generate liquid water. This requirement is critical for steady fog layers and can generally be met for all life cycles of a radiation fog, in that at its early stage, cooling dominates near the ground due to strong cooling of the surface, while at its mature stage when the fog is deepening, the strong cooling dominates in the upper levels due to the radiative cooling of large droplets at the fog top. Although there is little warming near the surface in a dense fog, the overall thermodynamic status is a cooling regime in the dense fog. As the overall thermodynamics inside the fog layers goes from cooling to warming, the fog will burn off. This is particularly true after sunrise.

The second condition required for keeping a steady fog is that the square bracketed term on the right hand side of (40) for shallow fog or of (50) for deep fog must be positive. For a steady shallow fog, the following condition should hold:

$$\int_0^1 (1-x)^{1/2} dx - \frac{2\delta}{H} \int_0^{H/\delta} \frac{dt}{1+e^t} > 0 \qquad (53)$$

Integration of (53) gives rise to the following inequality:

$$\frac{H}{3\delta} > \ln\frac{2e^{H/\delta}}{1+e^{H/\delta}} \tag{54}$$

Or

$$e^{H/3\delta} > \frac{2e^{H/\delta}}{1+e^{H/\delta}} \tag{55}$$

The inequality can be re-arranged as following cubic inequality:

$$r^3 - 2r^2 + 1 > 0 \tag{56}$$

where $r = e^{H/3\delta}$. The approximate solution for (56) is *r > 1.62*, or $\delta / H < 0.69$. That means if the characteristic FBL depth increases to 70% of the fog layers, the fog will become unstable and disperse. Therefore, besides a positive cooling rate, the following inequity is the second balance condition for a steady fog:

$$\delta < 0.69H \tag{57}$$

Similarly for a deep fog, the following inequality can be derived from equation (50):

$$r^3 - 2r^{1.83} + 1 > 0 \tag{58}$$

The approximate solution for (58) is r > 1.4 , or $\delta / H < 1.0$. That means if the characteristic FBL depth reaches the top of a deep fog, it will disperse. So the following condition is for a deep fog:

$$\delta < H \tag{59}$$

Combining both cases, $\delta < H$ is the balance condition for both shallow and deep steady radiation fogs. It can be easily tested that, if $\delta \to H$, the average LWC and *W(z)* at all levels will approach zero.

f. Critical turbulence exchange coefficient

Since δ depends on the turbulence exchange coefficient, substituting the second condition into the definition of δ in (38) or (49), critical turbulence exchange coefficients can be obtained for shallow and deep fogs respectively:

$$k < k_c = 1.38(\alpha\beta C_o)^{1/2} H^{3/2} \qquad \text{for a shallow fog} \qquad \text{(60-a)}$$

$$k < k_c = 1.41(\alpha\beta C_t)^{1/2} H^{3/2} \qquad \text{for a deep fog} \qquad \text{(60-b)}$$

To persist a steady fog, the inequity (60-a) or (60-b) for turbulence must be satisfied. The equations (60-a) and (60-b) demonstrate that the critical turbulence coefficients for shallow and deep fogs are $\sim C_o^{1/2}$ or $C_t^{1/2}$, and $\sim H^{3/2}$. It appears that k_c is more sensitive to the fog depth H than to the cooling rate, because (i) the fog depth may vary 100 times during its life time from its shallow stage to its mature stage, and (ii) H has a larger order of power (3/2) than that of the cooling rate (1/2). Like characteristic FBL depth, the critical turbulence coefficient is also a function of temperature, pressure, cooling rate, droplet gravitational settling and fog depth. The larger the cooling rate or the deeper the fog, the larger the critical turbulence exchange coefficient. The inequalities (60-a) or (60-b) indicate that the critical turbulence exchange coefficient defines the upper limit of turbulence that a steady fog can withstand and explains the roles of turbulence in both shallow and deep fogs. The initial patchy fog forms within 1~10 m of the surface and usually remains stable for a long time (conditioning), during which the surface turbulence must satisfied with a balance condition $k < k_c$, otherwise, the patchy fog will not be stable and the conditioning phase can not be completed before sunrise. Several factors are believed to contribute to the breakdown of such a balance: (1) local clouds moving over the fog region which will prevent outgoing net radiation from the ground and reduce the cooling inside the shallow fog; (2) warm advection; and (3) increasing local winds. All three factors will result in $k > k_c$, breaking the balance condition (60). In the first or second instance, a decrease in cooling rate leads to a decrease in k_c so that condition (60) can be broken. In the third instance, an increase in wind speed resulting in a larger k also leads to the breakdown of condition (60). Many observations and models have revealed the fact that increasing turbulence hinders the formation of fog but explained such a process with the dew mechanism. The dew mechanism only explains whether or not a fog forms, while condition (60) predicts whether an existing shallow fog is stable or not. A long-lasting stable shallow fog preludes the development of a deep fog.

A deep fog with a large H has a large k_c, implying that it is not easy for turbulence to disperse a deep fog since it requires strong turbulence to break the balance. Various k_c values for different H values, and different cooling rates at different temperatures are plotted in Figs. 7a-c.

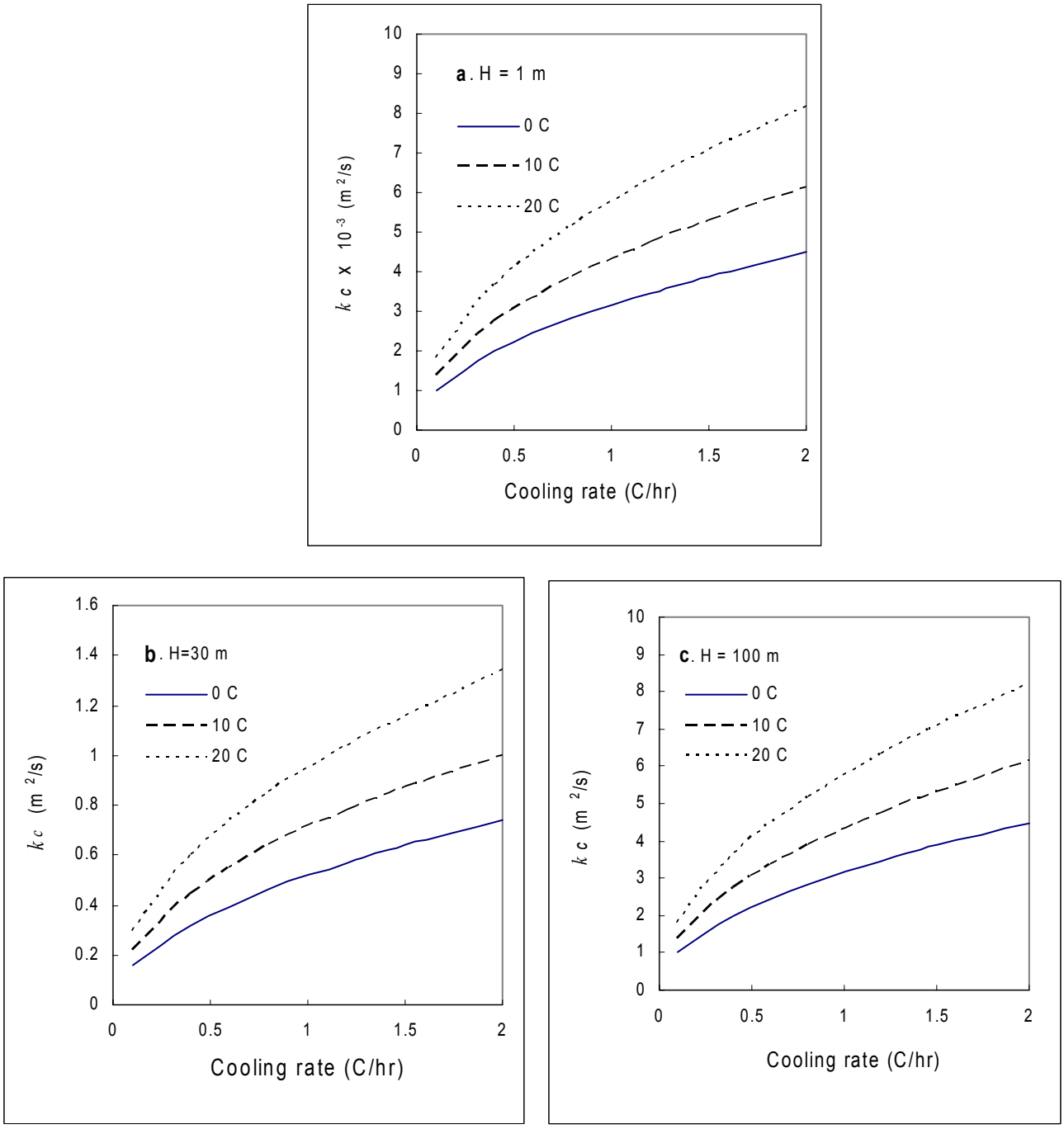

Fig. 7. Critical turbulence coefficients versus different cooling rates and temperatures for different fog top H: (a) *H = 1 m*, (b) *H = 30 m*, and (c) H = *100 m*.

k_c can be used as a threshold for checking whether a fog forms or whether it is in its dissipation stage. For example, for a patchy ground fog with a cooling rate ~ 1 $^oC\ hr^{-1}$ and $H \sim 1\ m$, Fig. 7a shows that k_c is $3\text{x}10^{-3}\ m^2s^{-1}$. That is, if turbulence near the surface drops below $3\text{x}10^{-3}\ m^2s^{-1}$, the fog can form, otherwise, the fog does not form or will quickly disappear, which is identical to the general turbulence intensity observed in the formation phase of a radiation fog (Roach 1976). However, for a deep fog with H ~100 m, k_c is 3 m^2s^{-1} (Fig. 7c). That means a 100m deep fog will disperse only when turbulence within the fog layers exceeds $3\ m^2s^{-1}$.

The role of the critical turbulence exchange coefficient in radiation fog can be conveniently explained with a *k_c-H state schematic diagram* (Fig 8). The diagram is divided according to the k_c curve into two regimes: $k < k_c$ (to the right of the k_c curve, or in the light blue region) where it is possible for fog to form; and $k > k_c$ (to the left of the k_c curve, or in the light green region) where it is impossible for a fog to form. The line H_s is the border which separates the upper unsaturated air and lower saturated air. Since the saturation begins at the ground and expands upward as cooling continues, the line H_s represents the upward-moving saturation front and the fog top is limited to below H_s. Point B is the intersection between the k_c curve and the saturation front line. Obviously, when the actual turbulence exchange coefficient is larger than k_B (or to the right of point B) there is no fog, while if the actual turbulence exchange coefficient is less than k_B (or to the left of point B), for instance at k_1 (which has two intersection points A and C), a steady fog will appear but the fog top is restricted to the tiny shaded area enclosed by A, B and C as shown in Fig. 8. As can be expected, the smaller k_1 is, the lower the point C is and the lower fog top can be. If turbulence does not cease completely, it is very difficult for a fog to form or stay stable on the ground. In an environment with larger turbulence, radiation fog is prone to initially form at a higher level then diffuse downward the ground since it is impossible for a fog top to initially appear at a level below point C. This might partially explain why radiation fog sometimes forms aloft.

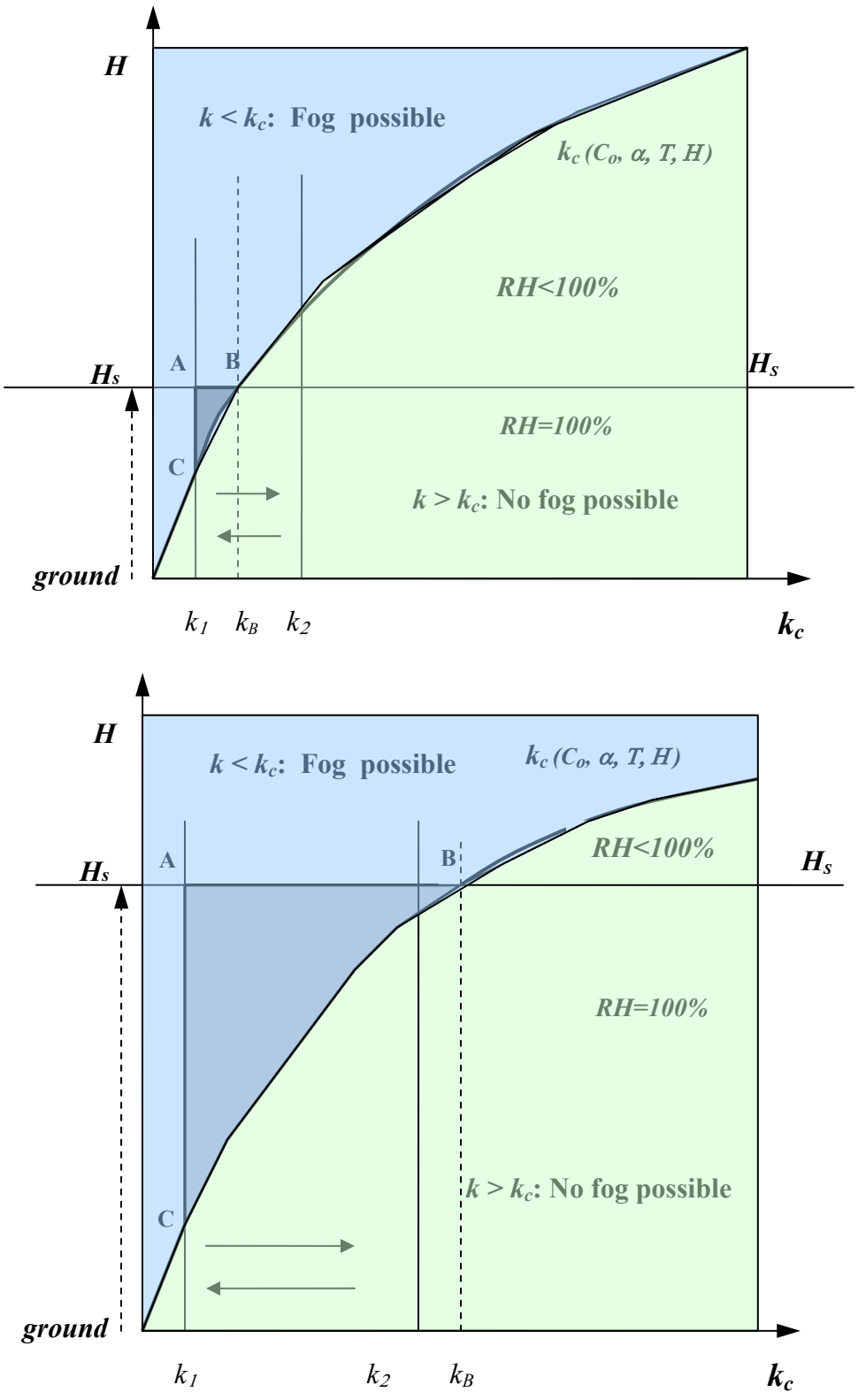

Fig. 8: k_c-H schematic diagram for a shallow fog (upper) and a deep fog (below).

After a fog forms, the conditioning stage begins. Its persistence relies on the subsequent status of surface turbulence. In general, the turbulence in a nocturnal boundary layer is weak but often has quasi-periodic oscillations with time (Roach 1976, Jiusto 1980). It is believed that these fluctuations in nocturnal turbulence cause, at least partially, oscillations of fog layers. The mechanism of how fluctuating turbulence affects fogs also can be explained by the k_c-H state schematic diagram. For instance, if the actual turbulence exchange coefficient k fluctuates between k_1 and k_2, across k_B of point B as shown in Fig. 8, the fog will fluctuate over time too. When k increases above $k_{B,}$, the fog is not stable and will disappear, while if k decreases below k_B a steady fog resumes. When the saturation front stays stable for a long time, the surface shallow fog will be stable and persist for a long time too. The scenario at the low end of k_c explains what was observed in patchy ground fogs or shallow fogs (Roach 1976, Meyer 1990). During this pre-fog or shallow fog stage, if the saturation front H_s steadily rises to a higher level, (e.g. due to the large droplet radiative cooling or upward diffusion of moist air near the fog top), k_B will increase which results in a larger shaded area as shown in the diagram. Consequently, the fog layers can endure stronger turbulence. This also explains why turbulence only dissipates shallow fogs, not dense fogs (Fitzjarrald 1989). The observations have shown that stronger turbulence helps to broaden the droplet distribution spectrum in radiation fog (Gerber 1981), if turbulence becomes larger but not large enough to exceed k_B (i.e. the variability range of the turbulence exchange coefficient k_1~k_2 on the left side of k_B as is shown in the diagram) it has a positive impact on the generation of large droplets at the fog top. The large droplets in turn produce the stronger radiative cooling which further lifts the fog top upwards. Since $k_c \sim H^{3/2}$, as H_s lifts higher the motion of the intersection point B towards the right will speed up and so will the fog top, causing a faster transition of fog layers to a deep fog. This implies that if a fog forms aloft, it is more likely to become a dense fog. This may explain why some fogs rapidly became denser just after sunrise. The behavior of the high end of k_c explains the fact that a growing dense fog was associated with increasing turbulence, and it also explains why the transition from the shallow stage to the mature stage is very fast as was observed in many deeper radiation fogs.

4. Accuracy and uncertainties

The errors and uncertainties of the LWC formulations in steady fogs, achieved from the asymptotic analysis, arise from following aspects. First, equation (9) was established under several assumptions, including steady conditions, horizontal homogeneity in fog layers, static and uniform

pressure and temperature in the computation of condensation, no scavenging effect from the surface vegetation, etc. All of these simplifications bring errors or uncertainties to the LWC solution. It is not appropriate to apply these formulations to a very unstable radiation fog nor to a fog over complex terrain. Second, the distribution formulations (39) or (46) are an asymptotic solution for the LWC equation with an accuracy of *O(k),* or the first-order of approximation of turbulence. If turbulence becomes strong, the solution is less precise. Since strong turbulence usually develops in a deep fog or during the dissipation stage of a radiation fog, the accuracy of the asymptotic solution appears lower for deep fogs than that for shallow fogs.

Besides the solution accuracy, the uncertainties in the input parameters also affect the estimation of liquid water content. The two key parameters in the asymptotic formulations are the cooling rate and the turbulence exchange coefficient. The accurate estimation of cooling rate directly affects the accuracy of the results, particularly for deep fogs. In a deep fog, the cooling rate may not be a constant distribution, and the formulation with a linear distribution of cooling rate should be applied. However, as was shown in the previous sensitivity test, the vertical LWC distributions computed with a constant or a linear cooling rate have no significant differences except for slightly different maximum LWC values, so the formulation with a constant cooling rate can be substituted without significant error if the cooling rate at the upper levels is not available.

The estimation error for turbulence intensity also has an impact on the turbulence term of the formulations. As we know, there are still many uncertainties in turbulence under very stable conditions because of the breakdown in turbulence structure. Most computations of the turbulence exchange coefficient in a surface layer have been based on a so-called "constant flux layer" assumption or similarity theory. However, the "constant flux layer" assumption may not hold under very stable nocturnal conditions, although some improvements have been made in the nocturnal boundary layer in numerical simulations of radiation fog (e.g. Duynkerke 1991, Bergot 1994).

Another defect in the asymptotic formulation is that the turbulence exchange coefficient is assumed to be constant with height. For optically shallow fog, which has a simple turbulence structure and is relatively passive without much interaction between the fog layers and environment, this assumption may be effective. But for a dense fog in which turbulence develops, the constant turbulence exchange coefficient may not be a good representation. Fortunately, as was discussed in the previous section, turbulence has less impact on the LWC in a dense fog than in a shallow fog; as

a result, in dense fogs the impact on the LWC from error in the turbulence will not be significant, which also reduces the impact of the accuracy problem in the solution.

The purpose of precisely estimating turbulence is to obtain an accurate value of the turbulence term in the asymptotic solution which is parameterized with the characteristic FBL depth. As has been discussed, the FBL bears some resemblance to the temperature-defined unstable surface mixing layer in real fogs. A practical question is: is it possible to use the depth of a surface unstable mixing layer to replace the characteristic FBL depth in the LWC computation? This question still can not be answered in the present study and needs more observations. But if the answer is positive, or it can be proved that there exists some explicit relationship between the characteristic FBL depth and the unstable surface mixing layer depth inside a radiation fog, then the temperature profile is the only requirement to estimate a vertical distribution of LWC in a steady radiation fog, which will be much simpler than LWC distributions from the unreliable estimation of a turbulence exchange coefficient in the nocturnal boundary layer. Likewise, if the critical turbulence exchange coefficient or characteristic FBL depth are not certain enough to use in the examination of the balance conditions for a steady fog, the surface unstable mixing layer depth determined from temperature profiles could also be substituted.

In addition to the uncertainties in turbulence and cooling rate, fog depth is another source of error since it is hard to determine without special measuring equipment. For patchy or shallow fogs, it is not difficult to find the fog top. But for deep fogs, the fog top is usually not convenient to find. One solution is to estimate it using relative humidity or dew point temperature profiles from a radiosonde or a numerical model.

5. Potential application in the operational forecast

Operational forecast of fogs so far has progressed little although some attempts to predict land fogs have been made with mesoscale models. Currently, the methodology of forecasting fog is either with a mesoscale model (e.g. Ballard 1991, Pagowski 2004) or with an one-dimensional column fog model nested on a regional model (e.g. Guedalia 1994, Muller 2005, Bergot 2005 among others). The forecast of fog is nothing but the forecast of its formation, dissipation and its average features of the LWC which solely determines the surface visibility ranges. The LWC formulation and balance criteria for steady fogs achieved in the present study seems to be an alternative way to forecast radiation fogs. More encouraging from the present study is that the examination of the

equilibrium conditions of a steady radiation fog is much less timing-consuming than forecasting the detailed processes of a radiation fog. For example, by evaluating the total cooling rate and the characteristic depth of the FBL or the turbulence strength at a few of the lowest model levels, forecasting fog could become a diagnostic procedure in the model's post processing.

6. Summary remarks

With the singular perturbation method, the simplified LWC equation for an equilibrium state in radiation fog was asymptotically solved in the first-order approximation of turbulence. The asymptotic and analytical formulation explicitly describes the vertical LWC structure, the self-maintenance mechanism and dynamical balance inside a steady radiation fog; the cooling is what produces fog liquid water, and the droplet gravitational settling is a regulator that adjusts the produced liquid water. Underestimation of the droplet gravitational settling will lead to an unrealistically high LWC magnitude. Turbulence is always a consumer of produced liquid water, however, the impact of turbulence on the LWC is less important for deeper fogs than that for shallow fogs. The solution also illustrates that for weak turbulence intensity the influence of turbulence is significant only near the ground, while as turbulence becomes stronger its influence can reach higher levels. Very strong turbulence may disperse entire fog layers.

The asymptotic solution reveals that there exists a turbulence sub-layer or fog boundary layer (FBL) near the surface inside a radiation fog. The characteristic FBL depth in a radiation fog is usually shallow for a large cooling rate and weak turbulence, while as the cooling rate decreases or turbulence increases the FBL becomes deeper. Such a LWC-defined turbulence sub-layer from the asymptotic solution represents, to some extent, the behavior of the developed surface mixing layer detected in mature fogs. When the characteristic FBL depth reaches the upper levels of a steady radiation fog, the balance within the fog is broken and the fog will disperse.

A critical turbulence exchange coefficient for steady radiation fog was discovered from the asymptotic solution. The critical turbulence exchange coefficient is a function of cooling rate and fog depth. More importantly, it defines the strongest turbulence intensity a radiation fog can endure, which can be used as a criterion to diagnose the formation or dissipation of radiation fogs. If the turbulence is less than this threshold in saturated air near the ground, a balance can be established for a patchy ground fog. If a patchy ground fog forms aloft, it maybe a precursor for a dense fog because it can withstand stronger turbulence which can effectively broaden the droplet spectrum and

promote the development of the fog bank. After a fog forms, the thicker the fog is the more turbulence it can endure and the longer it can last. But if turbulence increases to exceed this criterion, the fog will be unstable and disperse. The scenario for such a mechanism can be illustrated with a k_c-H state schematic diagram to explain the formation of fog aloft, the fluctuation of fog layers under the influence of oscillations in turbulence, and the growth of fog associated with turbulence. It should be noted that the concepts of FBL and the critical turbulence exchange coefficient for radiation fog are first introduced in the present study and were examined with only a limited number of observation cases. Their roles and impacts on radiation fog await further verification with more observational data.

The errors for the asymptotic solution were analyzed in terms of solution accuracy and uncertainties of the input parameters. An application of the asymptotic formulation requires a precise measurement or estimation of the cooling rate and turbulence strength in fog layers. For deep fogs, where the cooling rate at the fog top is usually not available, its estimation near the surface is a possible substitute. The asymptotic solution has an accuracy of the first-order approximation of turbulence, so the solution is less accurate for deep fogs than for shallow fogs because strong turbulence may develop within the deep fog. Fortunately, the influence of turbulence on deep fogs is much smaller than on shallow fogs. Because of the uncertainties in turbulence under very stable conditions, using the surface unstable layer depth (obtained from reliable temperature profiles) to replace the characteristic FBL depth was suggested in the LWC computation. But such an approach needs verification with more observations. If it is proved to be feasible, the computation of LWC in a steady radiation fog using only temperature profiles will be much more convenient.

REFERENCES

Ballard, S. P., B.W. Golding and R. N. B. Smith, 1991: Mesocale Experimental Forecasts of the Haar of Northeast Scotland, *Mon. Wea., Review*, **119**, 2107-2123.

Bergot, T. and D. Guedalia, 1994: Numerical forecasting of radiation fog. Part I: Numerical model and sensitivity tests. *Mon. Wea. Rev*., **122**, 1218-1230.

_____, D. Carrer, J. Noilhan and P. Bougeault, 2005: Improved site-specific numerical prediction of fog and low clouds: A feasibility study. *Wea. Forecasting*, **20**, 627-646.

Blackadar, A. K. and H. Tennekes, 1968: Asymptotic similarity in neutral barotropic planetary boundary layers. *J. Atmos. Sci*., **25**, 1015-1020.

Bott, A., U. Sievers, and W. Zdunkowski, 1990: A radiation fog model with a detailed treatment of the interaction between radiative transfer and fog microphysics. *J. Atmos. Sci*., **47**, 2153-2166.

Brown, R. and W. T. Roach, 1976: The physics of radiation fog: II – a numerical study. *Quart. J. Roy. Meteor. Soc*., **102**, 335-354.

Corradini, C. and G.Tonna, 1980: The parameterization of the gravitational water flux in fog models, *J. Atmos. Sci*., **37,** 2535-2539.

Croft, P. J., R. L. Pfost, J. M. Medlin, and G. A. Johnson, 1997: Fog forecsting for the southern region: A conceptual model approach. *Wea. Forecasting*, 12, 545-556.

____, and A. Burton, 2006: Fog during the 2004-2005 winter season in the northen mid-Atlantic states: Spatial characteristics and behaviors as a function of synoptic weather types. *12th Conference on Aviation, Range, and Aerospace*, Jan. 28- Feb 2, Atlanta, Amer. Meteor. Soc.

Duynkerke, P. G., 1991: Radiation fog: A comparison of model simulation with detailed observations. *Mon. Wea. Review*, **119**, 324341.

_____ , 1999: Turbulence, radiation and fog in Dutch stable boundary layers, *Boundary-Layer Meteor*., **90**, 447-477.

Fitzjarrald D. R. and G. G. Lala, 1989: Hudson valley fog environments. *J. Appl. Meteor*. **28**, 1303-1328.

Friedlein, M. T., 2004: Dense fog climatology, Chicago O'Hare international airport July 1996-April 2002. *Bull. Amer. Meteor. Soc*., April, 515-517.

Gerber, H. E., 1981: Microstructure of a radiation fog, *J. Atmos. Sci*., **38**, 454-458.

Glasow, R. V. and A. Bott, 1999: Interaction of radiation fog with tall vegetation, *Atmos. Environ*., **33**, 1333-1346.

Guedallia, D. and T. Bergot, 1994: Numerical forecasting of radiation fog, Part II: A comparison of model simulation with several observed fog events. *Mon. Wea. Review*, **122**, 1231-1246.

Jiusto, J. E., 1981: *Fog structure, Clouds: Their Formation, Optical Properties and Effects*, Edited by P. V. Hobbs and A. Deepak, Academic Press, 495 pp.

_____ , and G. G. Lala, 1980: Radiation fog formation and dissipation. A case study. *J. Rech Atmos*., **14**, 391-397.

Kelley W., 1994: Book Review: Introduction to the General Theory of Singular Perturbations. *Bull. Amer. Math*. Soc., **30**, 258-261.

Kunkel, B. A., 1984: Parameterization of droplet terminal velocity and extinction coefficient in fog models. *J. Climate Appl. Meteor*., **23**, 34-41.

Lala, G. G, E. Mandel and J. E. Jiusto, 1975: A numerical evaluation of radiation fog variables. *J. Atmos. Sci*.,32, 720-728.

Meyer, W. D. and G. V. Rao, 1999: Radiation fog prediction using a simple numerical model. *Pure Appl. Geophys*, **155**, 57-80.

Meyer, M. B. and G. G. Lala, 1990: Climatological aspects of radiation fog occurrence at Albany, New York. *J. Climate*, **3**, 577-586.

_____ , G. G. Lala, and J. E. Jiusto, 1986: Fog-82: A cooperative field study of radiation fog. *Bull. Amer. Meteor. Soc*., **67**, 825-832.

_____ , J. E. Jiusto and G.G. Lala, 1980: Measurements of visual range and radiation-fog (Haze) microphysics. *J. Atmos. Sci*., **37**, 622-629.

Meyer W. D. and G. Rao, 1999: Radiation fog prediction using a simple numerical model. *Pure Appl. Geophys*. **155**, 57-80.

Muller, M. D., M. Masbou, A. Bott, Z. Janjic, 2005: Fog prediction in a 3D model with parameterized microphysics. *World Weather Research Programme's Symposium on Nowcasting and Very Short Range Forecasting*, September 5-9, Toulouse, France.

Musson-Genon L., 1987, Numerical simulation of a fog event with a one-dimensional boundary layer model. *Mon. Wea. Review*, **115**, 592-607.

Oliver, D. A., W.S.Lewellen and G. G. Williamson, 1978: The interaction between turbulent and radiative transport in the Development of fog and low-level stratus, *J. Atmos. Sci*., **35**, 301-316.

O'Malley, R. E. Jr., 1974: *Introduction to Singular Perturbations*, New York, Academic Press, 206 pp.

Pagowski, M., I. Gultepe, and P.King, 2004: Analysis and modeling of an extremely dense fog event in southern Ontario. *J. Appl. Meteor*., **43**, 3-16.

Pinnick R. G., D. L Hoihjelle, G. Fernandez, E. B. Stenmark, J. D. Lindberg, G. B. Holdale, and S. G. Jennins, 1978: Vertical structure in atmospheric fog and haze and its effects on visible and infrared extinction. *J. Atmos. Sci*., **35**, 2020-2032.

Roach , W. T., R. Brown, S. J. Caughey, J. A. Garland and C. J. Readings, 1976: The physics of radiation fog: I – a field study. *Quart. J. Roy. Meteor. Soc*., **102**, 313-333.

_____, 1995: Back to basics: Fog: Part 2 -- The formation and dissipation of land fog. *Weather*, **50**, 7-11.

Rodhe, B., 1962: The effect of turbulence on fog formation, *Tellus*, **14**, 49-86.

Shuttleworth, W. J, 1977: The exchange of wind-driven fog and mist between vegetation and the atmosphere. *Boundary-Layer Meteor*., **12**, 463-489.

Taylor , G. I., 1917: The formation of fog and mist, *Quart. J. Roy. Meteor. Soc*., **43**, 241-268.

Tardif, R. , 2004: Characterizing fog occurrences in the northeastern United Sates using historical data. *11th Conference on Aviation, Range, and Aerospace*, Oct4-8, Hyannis, Amer. Meteor. Soc.

Turton, J. D. and R. Brown, 1987: A comparison of a numerical model of radiation fog with detailed observations. *Quart. J. Roy. Meteor. Soc*., **113**, 37-54.

Van Dyke, M. D., 1964: *Perturbation Methods in Fluid Mechanics*. New York, Academic Press, 229 pp.

Welch, R. M., M. G. Ravichandran, and S. K. Cox, 1986: Prediction of quasi-periodic oscillations in radiation fogs. Part I: Comparison of simple similarity approaches. *J. Atmos. Sci*, **43**,633-651.

Westcott, N., 2004: Environmental conditions associated with dense fog in Illinois. CD-Rom, *11th Conference on Aviation, Range, and Aerospace*, Oct4-8, Hyannis, Amer. Meteor. Soc.

Zdunkowski, W. G. and B. C. Nielsen, 1972: A radiative conductive model for the prediction of radiation fog, *Boundary Layer Meteor*., **2**, 152-177

Zhou, B., 1987: Numerical modeling of radiation fog. *ACTA Meteor. Sinica*, **45**, 21-29.